Research Article

A Numerical Approach to the Dynamic Response of the Deployment System during a Circular Cylinder Crossing through the Wave Zone

Xiaozhou Hu, Daojun Cai, and Yiyao Jiang

School of Mechanical and Electrical Engineering, Central South University, Changsha 410083, China

Correspondence should be addressed to Xiaozhou Hu; smallboathu@163.com

The dynamic response of the deployment system while deploying a circular cylinder crossing wave surface and the following submerging process are investigated numerically. The present numerical approach is based on the combination of solution methods of cable dynamics and computational fluid dynamics (CFD). For the implementation of the numerical approach, a cosimulation platform based on a CFD code and MATLAB is developed to study the fluid-solid interaction problem in the process. To generate regular waves, a numerical wave tank is built based on a piston-type wave generation method and a wave damping method applying porous media. Numerical simulations are performed based on the cosimulation platform. The sensitivities of cable tension, velocity, and acceleration of deployed body to different input parameters are investigated, including phase angles, wave heights, and periods of regular waves and deploying velocities, and the effects of those input parameters on dynamic responses of the deployment system are also discussed.

1. Introduction

In recent years, subsea working systems are widely used in such applications as marine resource development and utilization, maritime exploration, and survey [1–3]. To ensure the proper functioning of subsea working systems, the safe deployment or installation of them is one of the primary issues for marine and ocean engineers. When an offshore structure is deployed or launched into water, slamming occurs. Impulsive slamming loads lead to a nonlinear vibration of the deployment system, and the nonlinear effect which is enhanced because of the influence of waves would cause some problems, such as the slack cable phenomenon. If the operation of deploying cables is in frequently alternating taut-slack state, an exceptionally high tension in the cable will occur, which is also named as snap load because of its impact effect. In hostile ocean conditions, snap load would greatly increase the probability of missing of subsea structures. Moreover, the process of an offshore structure lowering through splash zone accompanies the interaction between the air, wave, and the rigid body, which is a complicated

fluid-solid problem, involving comprehensive consideration of time-varying hydrodynamic forces (slamming, drag, and inertia), buoyancy, vessel motion, waves, and possible snap loads in deploying cables. Therefore, to ensure a safe deployment of subsea working systems when they are lowered through the wave zone, it is essential to study the dynamic response of the deployment system with wave-solid interaction considered.

This paper mainly pays attention to the dynamic response of a deployment system while deploying a horizontal circular cylinder through wave zone for different deploying velocities and ocean conditions. In the wave impact and water entry process, offshore structures firstly impact on the wave surface, and then are gradually lifted from a dry state (in air) to partially immersed state and, eventually, to a wet state (fully immersed in water), which can be seen in Figure 1.

Hydrodynamic impact problems when solid bodies enter water have been investigated for nearly a century.

Pioneering researches performed by Karman [4], Wagner [5], Faltinsen [6], and others provided widely accepted theoretical basis. In the recent decade, researchers applied various
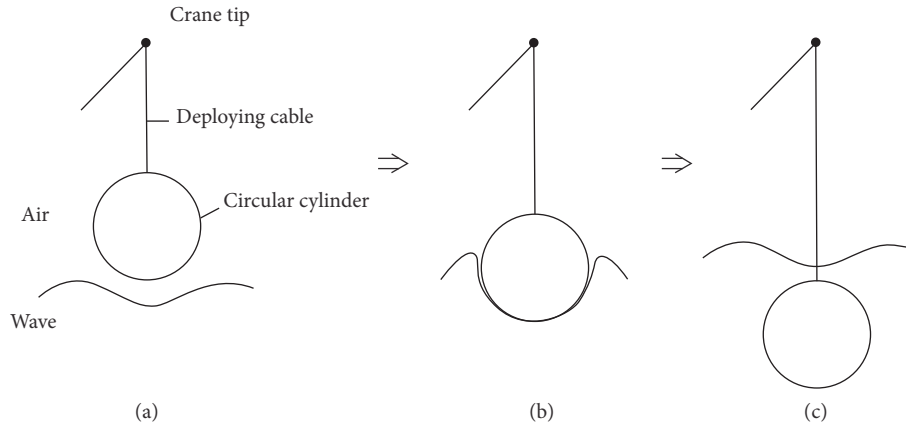
FIGURE 1: A circular cylinder lowering through the wave zone: (a) dry state; (b) partially immersed state; (c) fully immersed state.

theoretical or numerical methods for studying water entry of a circular cylinder, such as Sun and Faltinsen [7], Mnasri and Hafsia [8], Ghadimi et al. [9], Tassin et al. [10] and Iranmanesh and Passandideh-Fard [11]. However, as far as researches of deploying operation are concerned, these researchers were mainly devoted to investigating impact loads on rigid bodies and the deformation of water surface, with little attention paid to dynamic responses of the deployment or lifting system.

In recent years, remarkable progress in computer hardware and software technology and computational fluid dynamics (CFD) has greatly promoted researches in this field. For example, Buckner et al. [12], Bunnik and Buchner [13], and Bunnik et al. [14] applied an improved Volume of Fluid method to numerically predict wave loads during offshore structures in the splash zone. Zhang et al. [15] analyzed dynamic characteristics of the deployment system before and after water entry by using multibody dynamics (MBD) code Adams and CFD code Fluent, respectively; however, the dynamic response of deployment system during water entry process was not considered because MBD and CFD analysis were not integrated. W.-H. Wang and Y.-Y. Wang [16] simulated the physical process of a circular cylinder impacting on waves, and the response of lifting cable was obtained. Ryzhakov et al. [17] used a Particle Finite Element Method (PFEM) for simulations of the sea-landing of an unmanned aerial vehicle (UAV). Zhang et al. [18] investigated impact force acting on autonomous underwater vehicles when they contact with docks adopting commercial code Adams in conjunction with CFD software Fluent. Wen and Qiu [19] solved water entry problem by a constrained interpolation profile (CIP) method.

As mentioned above, the prediction of snap load which would result in highly nonlinear tension in deploying cables is very important; in this research field, Niedzwecki and Thampi [20], Thurston and Swanson [21], Lu [22], and others had made great contributions.

Many researchers utilized commercial software for ocean engineering to implement dynamic analysis of the deployment system, such as Orcaflex, SIMO, and SIMA. Selvåg [23] applied SIMO and Orcaflex to calculate wave impact forces on complex compression module in the splash crossing process, and comparisons between results obtained from numerical estimations and from model tests were made. Wu [24] carry out researches on the dynamic response of a template during the lifting operation through wave zone by SIMA program. Valen [25] modeled the lifting operation of ROV in the launching and recovery process, and results were compared with analysis based on DNV Recommended Practices. Gordon et al. [26] simulated the splash zone crossing process of suction pile using SIMO, and the sensitivity of cable tension to key parameters was presented. Jacobsen and Leira [27] developed a 1-degree-of-freedom dynamic system to estimate the tension acting in the lifting wire, and comparisons were made with the results obtained by SIMO. Li et al. [28, 29] simulated the lifting process of a monopole by the combination of an external Dynamic Link Library and SIMO program. Simulations performed by ocean engineering codes provided useful results; however, these commercial software programs are not based on CFD methods, and their failure to solve fluid-solid coupling problems during bodies lowering through wave zone results in the inability to consider the interaction between waves and deployed bodies; therefore hydrodynamic force on bodies and tension in deploying cables may be not well estimated.

This work is devoted to studying the dynamics of a cable-rigid body system during a circular cylinder lifting through wave zone with different deploying velocities and regular waves with different phase angles and wave heights and periods. Because vertical motion is much more important than motions of other directions for the deploying operation, the cable-rigid body system can be simplified as a 1-degree-of-freedom (1-DOF) mass spring system. For implementation, a cosimulation platform based on CFD codes Fluent and MATLAB is established [30], and calculations of 1-DOF system are performed by MATLAB, while wave related loads on bodies are estimated in a numerical wave tank generated by Fluent. Furthermore, sensitivities of cable tension and motion parameters of deployed body to regular waves and deploying velocities are also investigated.

The CFD numerical approaches will be firstly outlined, including governing equations, boundary conditions, wave generation, and absorption methods. Then, a number of numerical tests involving different deploying velocities and different waves are presented, and simulation results are discussed. Finally, conclusions are drawn in Section 5.

2. Numerical Methods

2.1. Governing Equations. For the motion of homogeneous and incompressible fluid, the continuity equation and Navier-Stokes equations are governing equations. Applying the Reynolds decomposition in N-S equations and averaging, the Reynolds-Averaged Navier-Stokes (RANS) equations can be derived:

$$\frac{\partial \rho}{\partial t} + \frac{\partial (\rho \overline{u}_i)}{\partial x_i} = 0 \quad (i = 1, 2)$$

$$\frac{\partial (\rho \overline{u}_i)}{\partial t} + \frac{\partial (\rho \overline{u}_i \overline{u}_j)}{\partial x_i} = -\frac{\partial \overline{p}}{\partial x_i}$$
$$+ \frac{\partial}{\partial x_j} \left[\mu \left(\frac{\partial \overline{u}_i}{\partial x_j} + \frac{\partial \overline{u}_j}{\partial x_i} \right) \right]$$
$$+ \frac{\partial}{\partial x_j} \left(-\rho \overline{u'_i u'_j} \right) + \rho \overline{f}_i, \tag{1}$$

where superscripts "$\overline{}$" stand for ensemble average of physical variables, u_i is the ith component of the velocity vector, ρ is the density of fluid, p is the pressure, μ is the dynamic viscous coefficient, f_i is body forces, and $-\rho \overline{u'_i u'_j}$ is the Reynolds stress tensor.

To fulfill turbulence closures for RANS equations, the standard k-ε turbulence model is applied in this work. Governing equations for the standard k-ε model are given by

$$\frac{\partial (\rho k)}{\partial t} + \frac{\partial (\rho k \overline{u}_j)}{\partial x_i} = \frac{\partial}{\partial x_j} \left[\left(\mu + \frac{\mu_t}{\sigma_k} \right) \frac{\partial k}{\partial x_j} \right] + \rho G_k$$
$$- \rho \varepsilon$$

$$\frac{\partial (\rho \varepsilon)}{\partial t} + \frac{\partial (\rho \varepsilon \overline{u}_j)}{\partial x_i} = \frac{\partial}{\partial x_j} \left[\left(\mu + \frac{\mu_t}{\sigma_\varepsilon} \right) \frac{\partial k}{\partial x_j} \right]$$
$$+ \frac{\varepsilon}{k} \left(C_{\varepsilon 1} \rho G_k - C_{\varepsilon 2} \rho \varepsilon \right) \tag{2}$$

$$\mu_t = \frac{C_\mu \rho k^2}{\varepsilon}$$

$$G_k = \frac{\mu_t}{\rho} \left(\frac{\partial \overline{u}_i}{\partial x_j} + \frac{\partial \overline{u}_j}{\partial x_i} \right) \frac{\partial \overline{u}_i}{\partial x_j},$$

where k is the turbulence kinetic energy (TKE), ε is the dissipation rate of TKE, μ_t is the eddy viscosity, and G_k is the production rate of TKE.

Referring to Launder et al.'s work [31], the empirical coefficients in (2) can be given as follows:

$$C_\mu = 0.09,$$
$$C_{\varepsilon 1} = 1.44,$$
$$C_{\varepsilon 2} = 1.92, \tag{3}$$
$$\sigma_k = 1.0,$$
$$\sigma_\varepsilon = 1.3.$$

To track the wave surface, the Volume of Fluid (VOF) method is employed. If the volume fraction of water and air in each cell is a_w and a_a, respectively, the capturing of the interface between different phases is achieved by the solution of a continuity equation for the volume fraction of liquid. This equation of a_w has the following form:

$$\frac{\partial a_w}{\partial t} + u_i \frac{\partial (a_w)}{\partial x_i} = 0 \tag{4}$$

$$a_w + a_a = 1. \tag{5}$$

For (5), $a_w = 0$ means gas phase, and $a_a = 0$ means liquid phase, while $a_a = 0\sim1$ means the mixture phase or interface between gas and liquid water.

For the solution of governing equations, appropriate boundary conditions at all boundaries of the domain should be defined. The boundary conditions which need to be satisfied are as follows: (1) the kinematic and dynamic free surface boundary conditions at the free surface; (2) the normal-flux boundary condition at the bottom of domain and the rigid body. Besides, for generating waves for studying dynamic problems described in this work, a numerical wave-maker and an artificial damping zone are put on the left and right wall boundary, respectively.

2.2. Wave Generation and Damping Methods. In this work, the wave generation is performed by a piston-type wave-maker. The schematic of a numerical wave tank with a piston wave-maker at the left wall boundary is given in Figure 2.

A paddle moves sinusoidally with the function:

$$X(t) = \frac{X_0}{2} \sin \omega t, \tag{6}$$

where X_0 is the maximum horizontal displacement of the paddle and ω is the angular frequency. The motion of the paddle generates a propagating wave which is composed of a regular incoming wave with wave number k and angular frequency ω and attenuating incident waves. With the attenuating components eliminated, surface elevation can be given by

$$\eta(x, t) = \frac{X_0}{2} \frac{4 \sinh^2 kd}{2kd + \sinh 2kd} \cos(kx - \omega t)$$
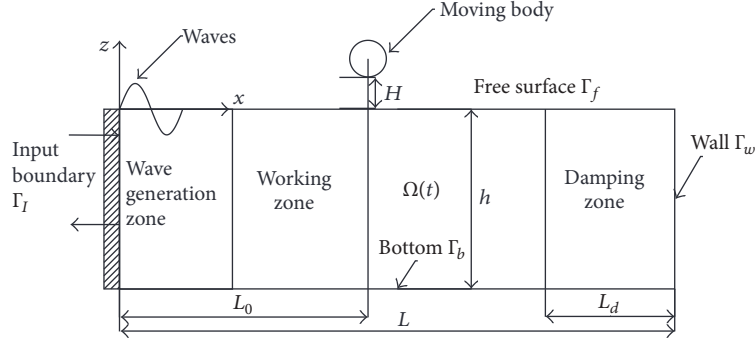$$= \frac{H}{2} \cos(kx - \omega t), \tag{7}$$

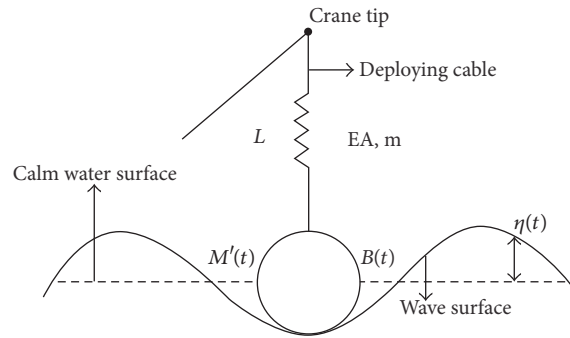FIGURE 2: Numerical wave tank and a moving body.

FIGURE 3: The cable-rigid body system.

where d is the water depth, k is wave number, and wave height H can be obtained by

$$H = \frac{4\sinh^2(kd)}{2kd + \sinh(2kd)} X_0. \tag{8}$$

It is necessary to absorb the attenuating incident wave so as to avoid the wave surface of the working zone being disturbed. In this work, at the right part of the flow domain, porous media are used to form an artificial damping zone so that reflected waves are gradually vanished along the direction of wave propagation. Porous media are modeled by the addition of a momentum source term to the standard fluid flow equations, which can be given by

$$S_i = -\left(\frac{\mu}{\alpha} v_i + C_2 \frac{1}{2} \rho |v_i| v_i\right), \tag{9}$$

where S_i is the source term for the ith (x, y or z) momentum equation, $|v_i|$ is the magnitude of the velocity, μ is the viscosity of the fluid, C_2 is the inertial resistance factor, and α is the permeability of porous media.

3. Simplified Analytical Model

Although the motion of a deployed body has six degrees of freedom of a rigid body, the predominant motion is vertical direction. Compared with accurate but time-consuming

multibody dynamics approaches, the 1-DOF dynamic system is more suitable for the present research. Therefore, it is fairly reasonable to assume that the cable-rigid body (circular cylinder) system can be simplified as a 1-DOF system, as shown in Figure 3.

Hu et al. [30] developed an analytical model to investigate the dynamic responses of deployment system during bodies impacting on initially calm water. In this paper, based on Hu et al. [30], an improved approach is presented so as to consider the influence of waves, which is briefly described as follows.

For the 1-DOF cable-rigid body system, if the deployed body has a vertical motion z relative to coordinate system fixed with space, the following equation can be obtained:

$$M'(t)\left(\frac{d^2 z}{dt^2} - \frac{d\eta}{dt}\right)$$

$$= Mg - B(t) - \rho V(t)\frac{d\eta}{dt} - T(t) \tag{10}$$

$$- 0.5\rho C_D A\left(\frac{dz}{dt} - \eta\right)\left|\frac{dz}{dt} - \eta\right| - F_s$$

and $M'(t) = M + A_{33}$, $B(t) = \rho V(t)g$, $\eta = \omega(H/2)\cos(kx - \omega t)$, and $F_s = (d/dt)[A_{33}(dz/dt - \eta)]$, where M is the mass of the deployed body in air, A_{33} is the time-varying heave added

mass of the deployed body, g is gravitational acceleration, $B(t)$ is the buoyancy force, ρ is density of water, $V(t)$ is the submerged volume of the deployed body, H and ω are wave height and frequency of regular waves, respectively, $T(t)$ is the tension that the cable acts on the deployed body, C_D is the drag coefficient, A is vertical projected area, and F_s is the slamming force.

Equation (10) can be rewritten as

$$M\frac{d^2z}{dt^2} = Mg - T(t) - F_{\text{hyd}}, \tag{11}$$

where F_{hyd} is hydrodynamic forces which can be obtained by

$$
\begin{aligned}
F_{\text{hyd}} = A_{33}\left(\frac{d^2z}{dt^2} - \frac{d\eta}{dt}\right) + \rho V(t)\left(g + \frac{d\eta}{dt}\right) \\
+ 0.5\rho C_D A\left(\frac{dz}{dt} - \eta\right)\left|\frac{dz}{dt} - \eta\right| + F_s.
\end{aligned}
\tag{12}
$$

Hydrodynamic forces F_{hyd} can be calculated by CFD codes. It is worth noting that both the time-varying buoyancy and drag force on the deployed body during water entry are included in hydrodynamic forces.

In the 1-DOF cable-rigid body system, the cable can be modeled as a linear spring; if the position of line end of the cable can be obtained, the elongation and thereby the tension on the cable can be determined. For more details, one can refer to the paper by Hu et al. [30].

The dynamic response of deployment system during a rigid body crossing wave zone is a complex fluid-structure interaction problem, which involves fluid dynamics, mechanical dynamics, and the coupling between them, and thus single solution methods have incapacity to deal with this problem. Therefore, a cosimulation platform is developed based on the CFD software Fluent and MATLAB, and this can also be referred to Hu et al. [30].

4. Dynamic Simulation and Analysis

4.1. Verification of Numerical Wave Tank.
To verify the effectiveness and accuracy of numerical wave generation and dissipation approaches presented in Section 2, a regular wave with wave height 2.5 m and period of 6 s is applied as the target wave. The permeability of porous media of the damping zone is given by

$$\frac{1}{\alpha(x)} = \alpha_0\left(\frac{x - x_s}{x_e - x_s}\right), \tag{13}$$

where α_0 is a constant permeability and x_s and x_e are the starting point coordinate and the ending point coordinate of the damping zone, respectively. Parameters used in simulations are as follows: $\alpha_0 = 1 \times 10^{-6}$, $x_e = 300$ m, $x_s = 150$ m, and calm water depth (d) = 30 m. Parameters of the numerical wave tank and locations of wave gauges are shown in Figure 4.

Wave surface elevations are probed at four locations ($x = 50$ m, 100 m, 200 m, and 300 m, as shown in Figure 4) of the numerical wave tank, and time histories of numerical wave

surface elevations are compared with those of the target wave, which are shown in Figure 5. In working zone of wave tank ($x = 50$ m, 100 m), a good agreement can be observed between simulation results and those of the target wave, while wave elevations in the damping zone ($x = 200$ m, 300 m) are close to zero, which means satisfactory wave energy-dissipation capacity is achieved. Therefore, it can be concluded that the wave generation and damping performance of the numerical wave tank is good and can meet demands of investigating the dynamic response of deployment system during a circular cylinder lowering through splash zone numerically.

4.2. Parameters of Dynamic Simulations.
A circular cylinder with neutral buoyancy is selected as the rigid body which is to be deployed by the deployment system, parameters of which are as follows: length $L = 10$ m, diameter $D = 2$ m, and thus mass $M = 31416$ kg. The unstretched length L_0 and initial stiffness K of the deploying cable are 10 m and 2000 kN/m, respectively.

To investigate the sensitivity of cable tension and motion parameters of the circular cylinder to regular waves and deploying velocities, different parameters are considered in simulations:

(1) Phase angle = $\{0°, 90°, 180°, 270°\}$.

(2) Wave height $H = \{1, 2, 2.5, 4\}$ (m).

(3) Wave period $T = \{2, 4, 6, 8\}$ (s).

(4) Deploying velocity $V_d = \{0.5, 1, 2, 4\}$ (m/s).

4.3. A Simulation Example of Water Entry Process of a Circular Cylinder.
A simulation example is used to reveal the whole process of water entry of the circular cylinder with considering the influence of waves. Main setups of this example are as follows: the radius of the circular cylinder R is 1 m, the target wave is a regular wave with wave height $H = 2.5$ m, and period $T = 6$ s; the deploying velocity V_d is 2.5 m/s; a dimensionless parameter $V_d\,t/R$ is defined, and $t = 0$ when the cylinder initially touches wave surface. Wave surface profiles at $V_d\,t/R = 0$, 0.5, 1, and 2 are shown in Figure 6. Figures can demonstrate the water entry process of the circular cylinder in waves, and time-varying free surface deformation can be clearly observed.

4.4. Influence of Wave Impact Phase Angles.
Wave impact phase angles can reflect the relative position between the rigid body and wave surface when impact occurs. Figure 7 shows different wave impact phase angles: positions marked 1, 2, 3, and 4 correspond to phase angles of 0°, 90°, 180°, and 270°, respectively. The regular wave on which the rigid body impacts is determined as wave with $H = 2.5$ m and $T = 6$ s. Besides, the case of the body lifting through initially calm water surface is also considered.
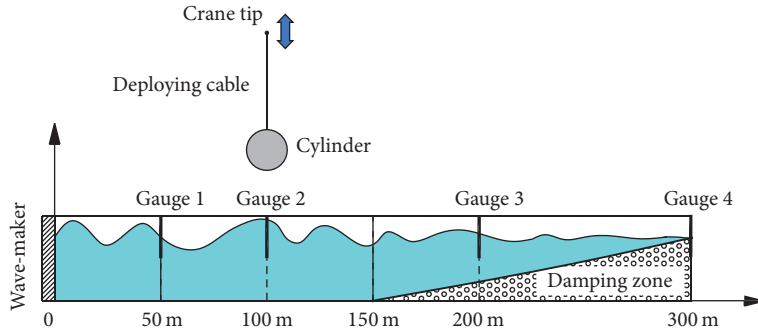
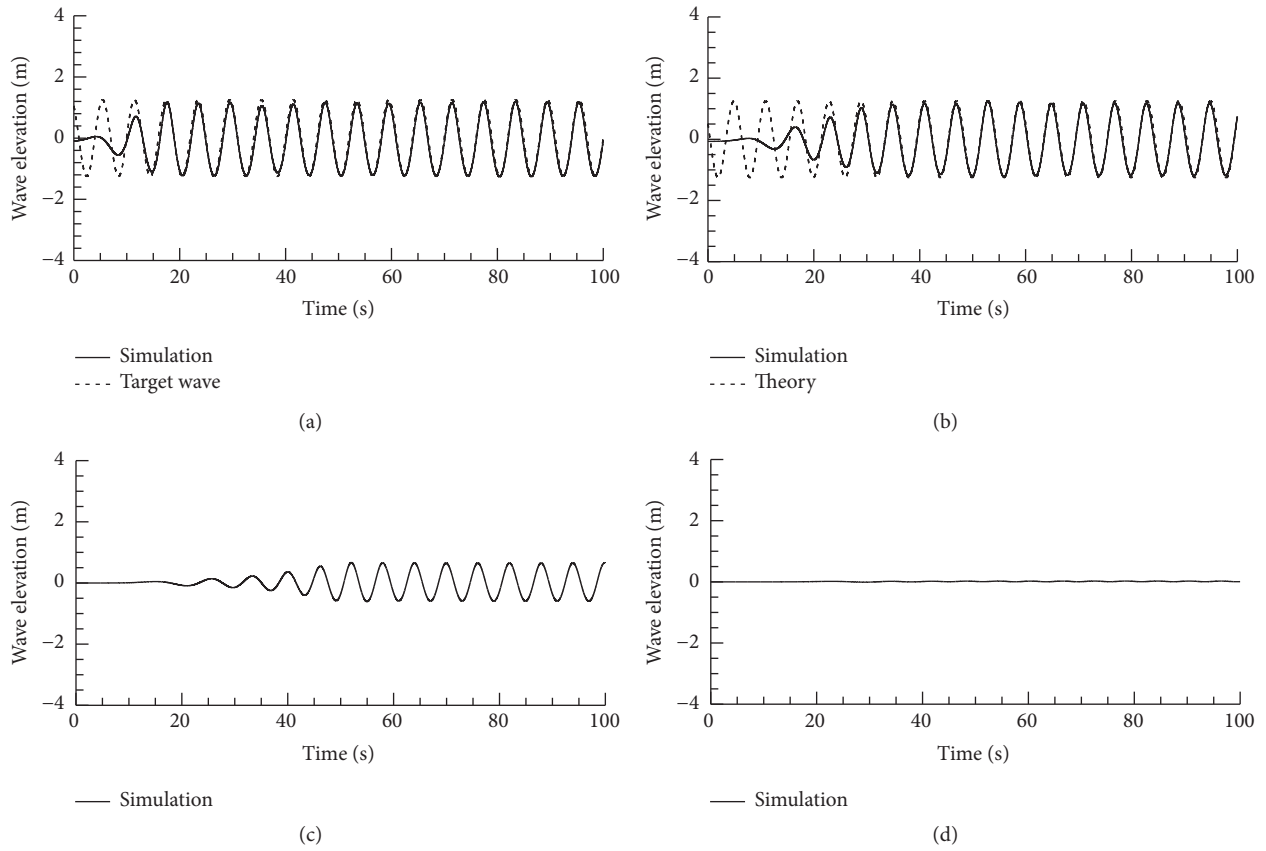FIGURE 4: A schematic of numerical wave tank.

FIGURE 5: Wave elevation at four different locations: (a) $x = 50$ m; (b) $x = 100$ m; (c) $x = 200$ m; (d) $x = 300$ m.
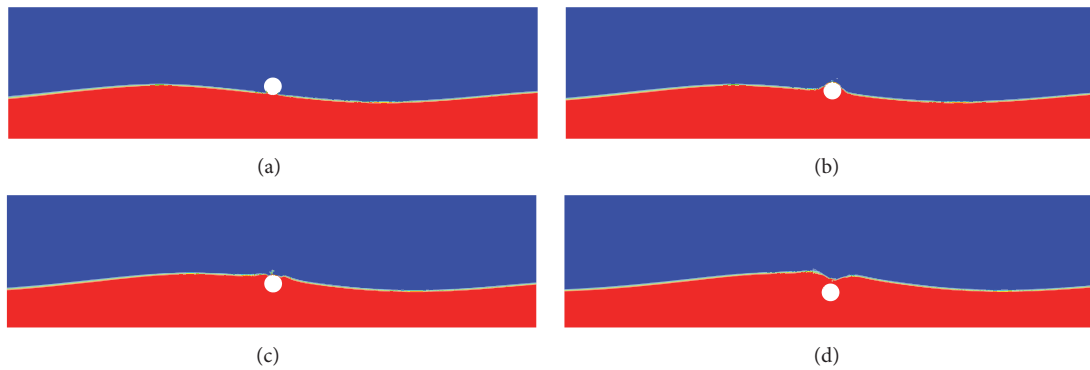

FIGURE 6: Water entry process of a circular cylinder: (a) $V_d t/R = 0$; (b) $V_d t/R = 0.5$; (c) $V_d t/R = 1$; (d) $V_d t\ t/R = 2$.
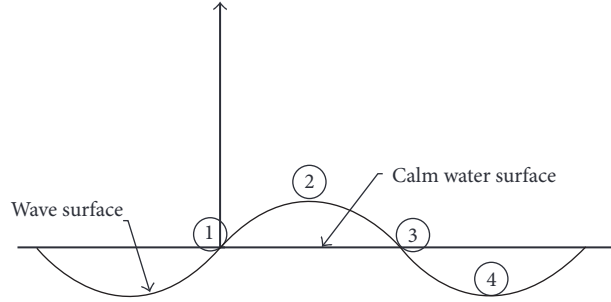
FIGURE 7: Wave impact positions.

From Figures 6(a)–6(c), 9(a)–9(c) and 10(a)–10(c), it can be seen that most of time history curves of velocity, acceleration of the body, and tension acting on the body have the characteristic of periodic but not harmonic oscillations. Applying $M = 31416$ kg and $K = 2000$ kN/m, the natural period of the cable-rigid body system can be calculated by

$$T_0 = 2\pi \sqrt{\frac{M}{K}} = 0.787 \text{ s}. \tag{14}$$

It can be seen that oscillating periods of cases are nearly approximate but bigger than the natural period, which is mainly due to the complex body-wave interaction.

From curves of tension, it is worth noting that some points or parts of curves are equal to zero; that is to say, cables of these cases are in a slack state, and the occurrence of this phenomenon is because the deploying cable is highly resistible to tension while could hardly bear compression. When the slack state appears, the cable exerts no influence on the motion of the deployed body, and this is a dangerous condition because control methods which play a role by means of the cable cannot make a difference in hostile ocean conditions. It can also be observed that an alternating slack-taut condition of the deploying cable emerges in some cases, including $V_d = 0.5$ m/s with 0° and $V_d = 1$ m/s with 180°, and if the transition rate at which the cable becomes taut from slack state is big enough, it may cause snap force which is preferably avoided. Although smaller deploying velocity means smaller slamming load, the idea that smaller deploying velocities are much safer than bigger ones is not absolutely correct; for example, the dangerous alternating slack-taut condition occurs when $V_d = 0.5$ m/s and $V_d = 1$ m/s, while it does not occur when $V_d = 2$ m/s.

Figures 8–10 also clearly illustrate that wave phase angles play an important role in determining the dynamic response of the cable-rigid body system: for all cases, the maximum upward acceleration appears at the moment just after wave impact occurs, and, compared with other phase angles, cases with 0° have the biggest acceleration, while cases with 270° have the smallest one. This phenomenon is mainly due to

the effect of wave slamming load. At the moment when wave impact occurs, buoyancy, drag force, and added mass are zero, and $T = Mg$, (10) can be rewritten as:

$$\frac{d^2z}{dt^2} = -\frac{F_s}{M}. \tag{15}$$

According to previous researches, the slamming force F_s on an object is mainly dependent on the relative velocity between it and wave surface; from this point of view, the cases with 0° have the biggest relative velocities while cases with 270° have the smallest one. Besides, curves of tension and velocity have the tendency similar to those of acceleration.

From the case of $V_d = 0.5$ m/s with phase angle = 270°, a special phenomenon can be seen: curves of tension, velocity, and acceleration are parallel to x-axis at the beginning, and it is because of the fact that the wave is receding faster than the body is being lowered and thus no slamming occurs.

4.5. Influence of Wave Height. Cases with four wave heights of regular waves—1 m, 2 m, 2.5 m, and 4 m—are considered, while periods of regular waves and deploying velocity are determined as 6 s and 1 m/s, respectively.

Figure 11 shows time histories of tension, velocity, and acceleration of the circular cylinder subjected to waves with different heights. On one hand, as a whole, with wave height increasing, the amplitude of variation of curves becomes much bigger. On the other hand, curves with smaller wave height are stable and nearly harmonic; with the wave height increasing, the curves are no longer harmonic but still are periodic. When wave height is 4 m, the minimum tension reaches zero, which means the deploying cable becomes slack; after a short period of time, the tension is larger than zero again, which means deploying cable becomes taut, and therefore the alternating slack-taut condition occurs, as mentioned in Section 4.4.

4.6. Influence of Wave Period. Cases with four periods of regular waves—2 s, 4 s, 6 s, and 8 s—are considered, while wave heights of regular waves and deploying velocity are determined as 2.5 m and 1 m/s, respectively.

Figure 12 shows time histories of tension, velocity, and acceleration subjected to waves with different periods. With
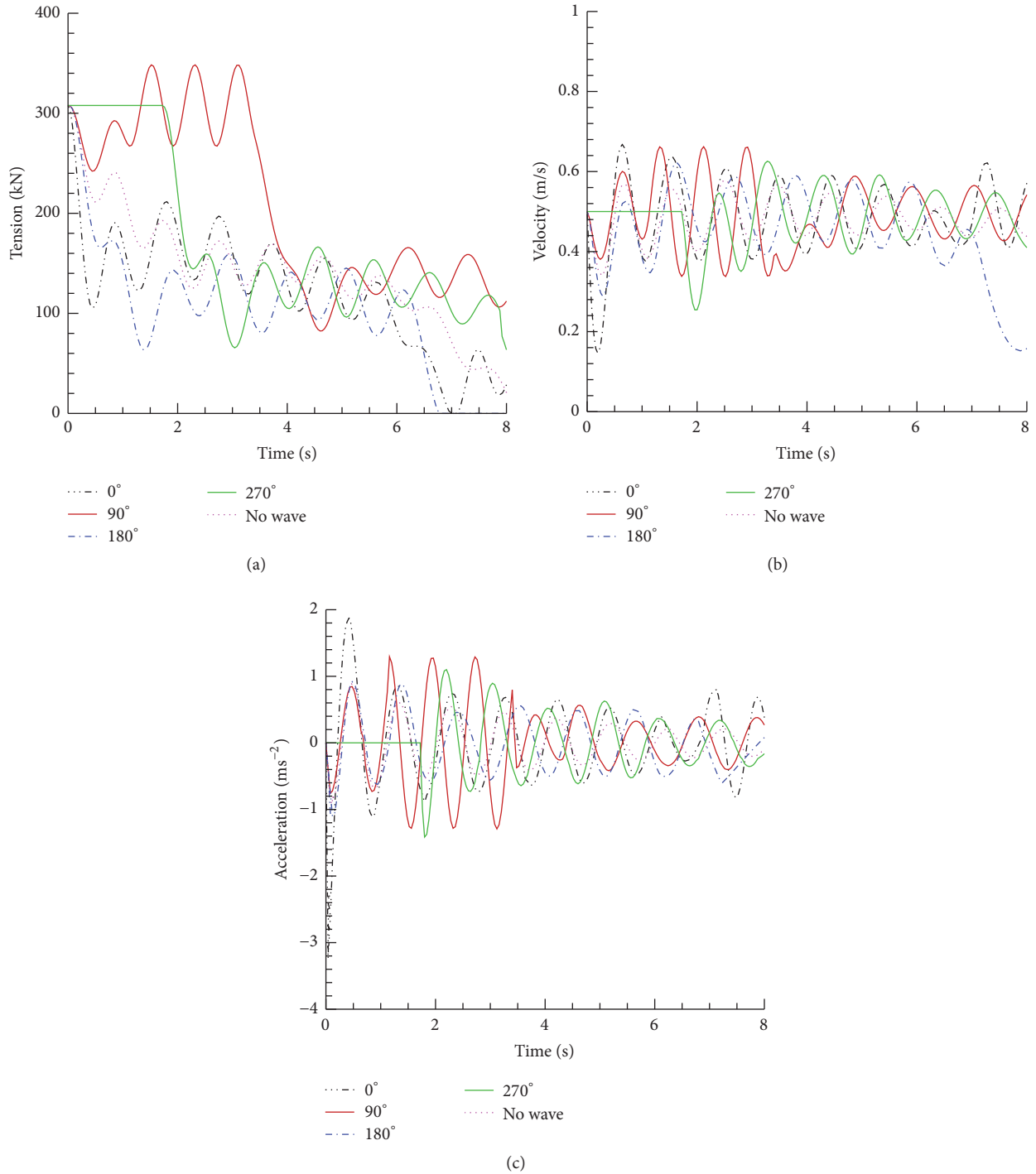
(a)

(b)

(c)

FIGURE 8: Influence of wave impact phase angles ($V_d = 0.5$ m/s): (a) tension acting on the cylinder; (b) velocity of the cylinder; (c) acceleration of the cylinder.

wave period increasing, the amplitude of variation of curves becomes much smaller. When wave period is 6 s and 8 s, curves are stable and nearly harmonic, and no slack condition can be seen. When wave period is 2 s or 4 s, the situation is different; for the case with $T = 2$ s, the alternating slack-taut condition occurs three times, and there are two local peak values of tension, and the first and the second one are 1.4 and 2.1 times bigger than the gravitational force of the deployed circular cylinder, respectively, which is a rather dangerous condition; for the case with $T = 4$ s, the alternating slack-taut
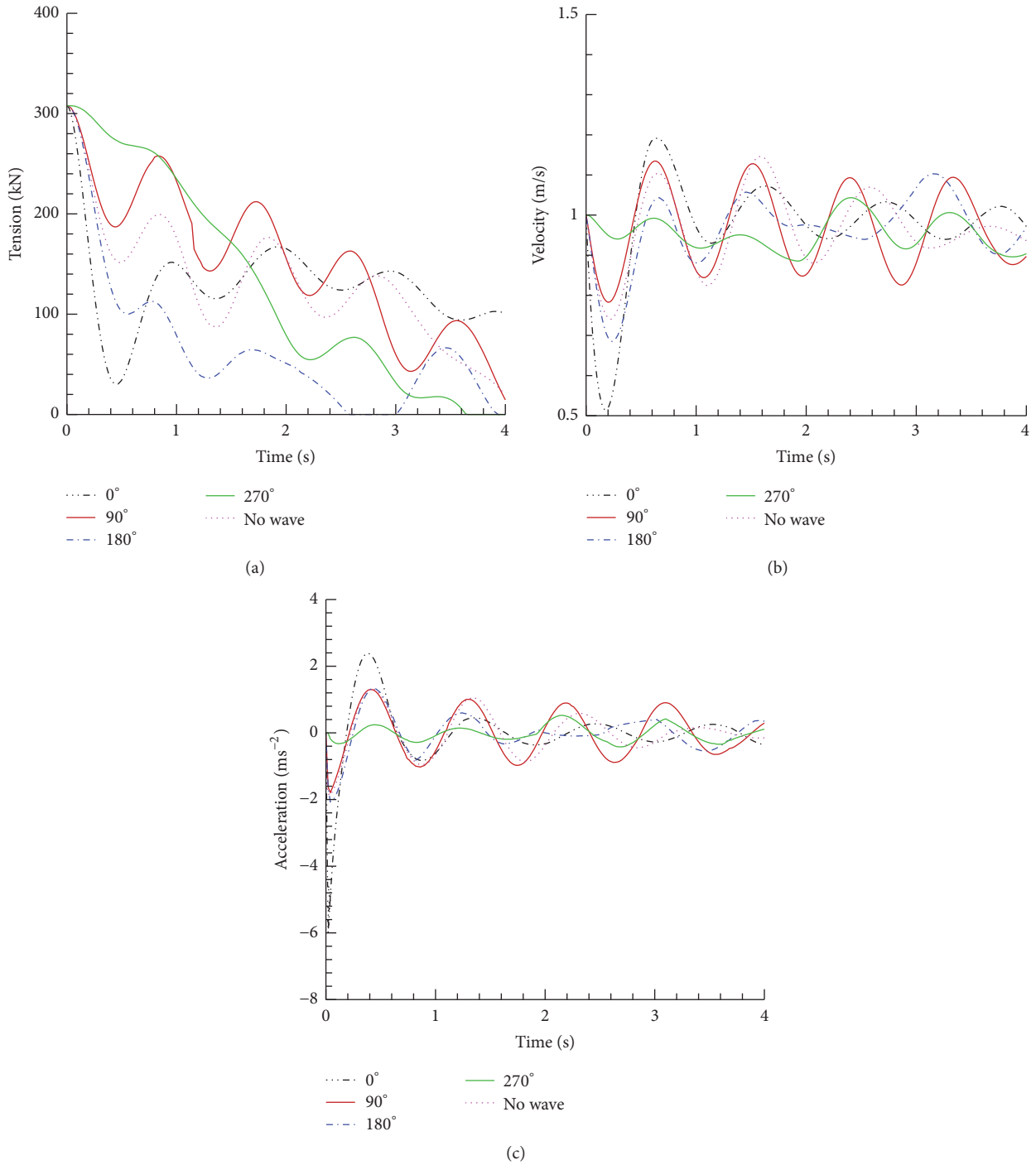
(a)

(b)

(c)

FIGURE 9: Influence of wave impact phase angles ($V_d = 1$ m/s): (a) tension acting on the cylinder; (b) velocity of the cylinder; (c) acceleration of the cylinder.

condition occurs once; however, the maximum tension is smaller than the gravitational force of the circular cylinder. Considering that the natural period of the cable-deployed body system T_0 is 0.787 s, it is reasonable to conclude that the alternating slack-taut condition is more likely to occur when wave period is closer to the natural period of the cable-rigid body system.

5. Conclusion

In this paper, the dynamic response of a deployment system during a circular cylinder lowering through wave zone is investigated numerically. A 1-DOF approach is applied to represent the dynamic cable-rigid body (circular cylinder) system. Numerical simulations are performed on
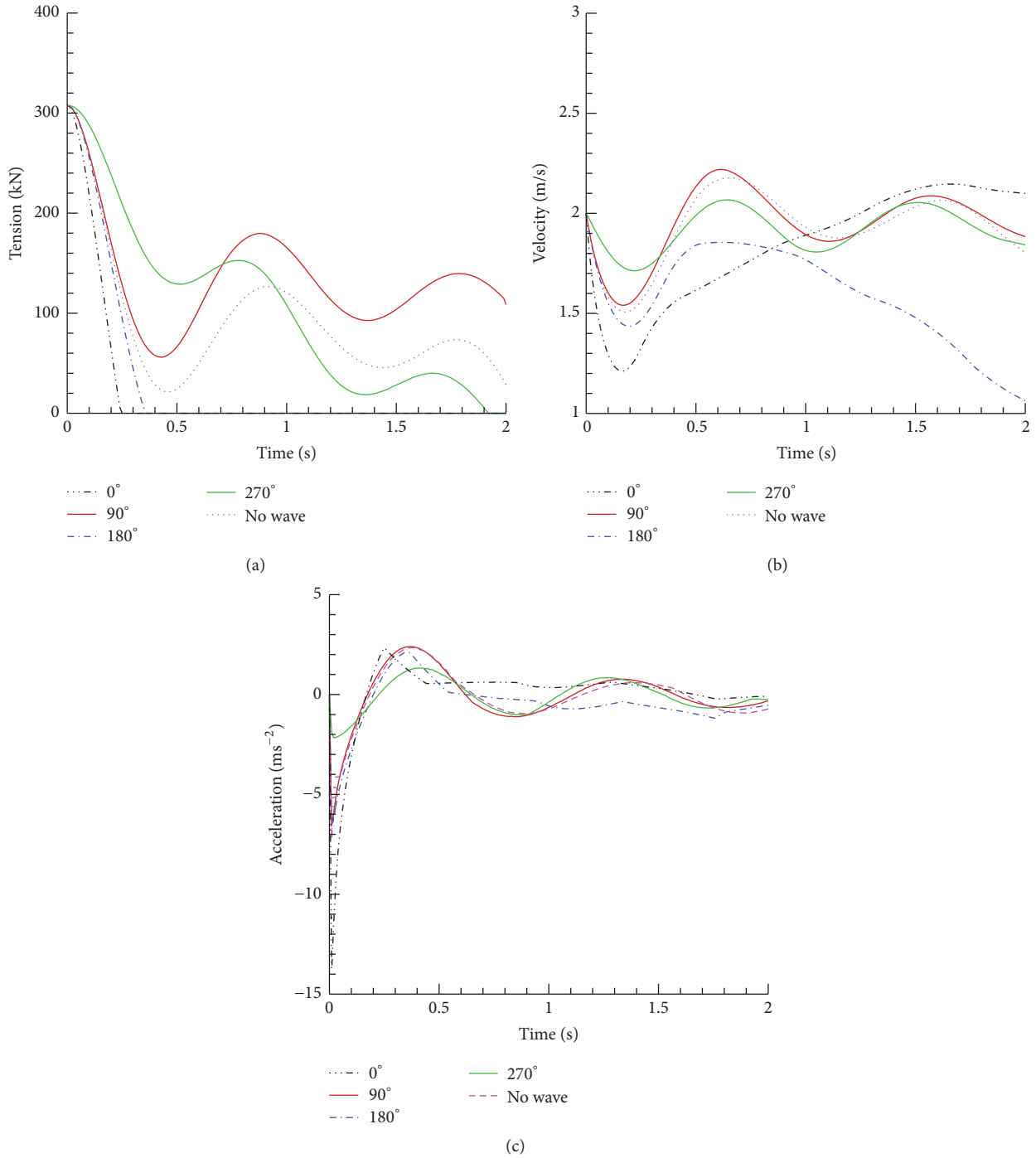
(a)

(b)

(c)

FIGURE 10: Influence of wave impact phase angles ($V_d = 2$ m/s): (a) tension acting on the cylinder; (b) velocity of the cylinder; (c) acceleration of the cylinder.

a cosimulation platform based on CFD code and MATLAB, which can generate regular waves and deal with fluid-solid coupling problems.

The following conclusions can be given, based on analysis of simulation results:

(1) A piston-type wave generation and porous media wave absorption methods are applied to generate

regular waves and verified by the comparison with the target wave.

(2) Cases with wave phase angle 0° have the largest amplitude of variation of curves and the biggest maximum acceleration, which is due to the largest relative velocity between body and wave. At some time points, the cable become slack, and an alternating slack-taut
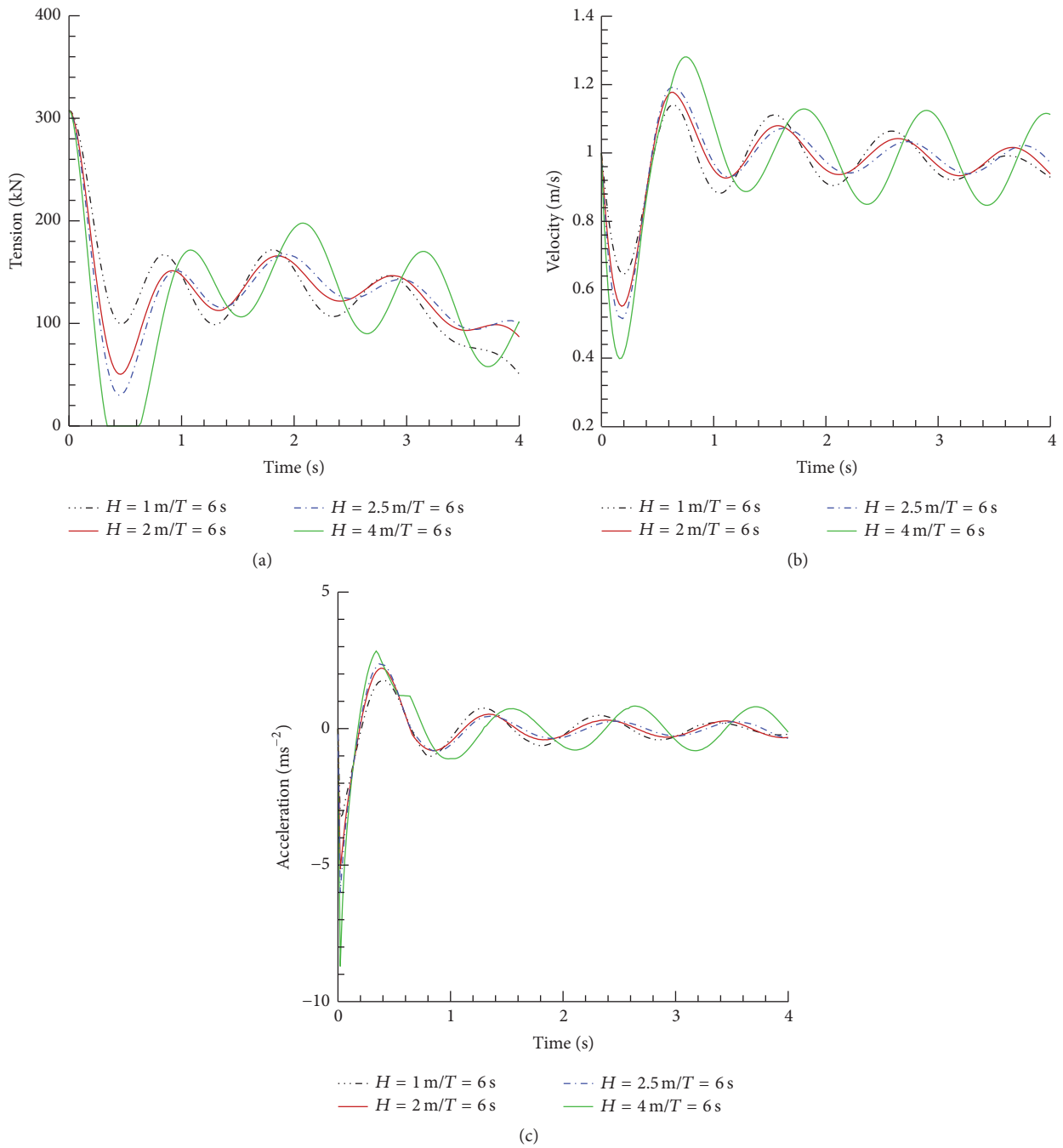
(a)

(b)

(c)

FIGURE 11: Influence of wave heights: (a) tension acting on the cylinder; (b) velocity of the cylinder; (c) acceleration of the cylinder.

condition of the deploying cable can be observed, which is preferably avoided.

(3) Except for some extreme situations, curves of velocity, acceleration, and tension of the circular cylinder oscillate periodically. With wave height increasing and wave period decreasing, the amplitude of variation of curves becomes bigger, and the alternating slack-taut condition occurs when wave height is large enough or wave period is close to the natural period of the dynamic system.

Conflicts of Interest

The authors declare that there are no conflicts of interest regarding the publication of this paper.
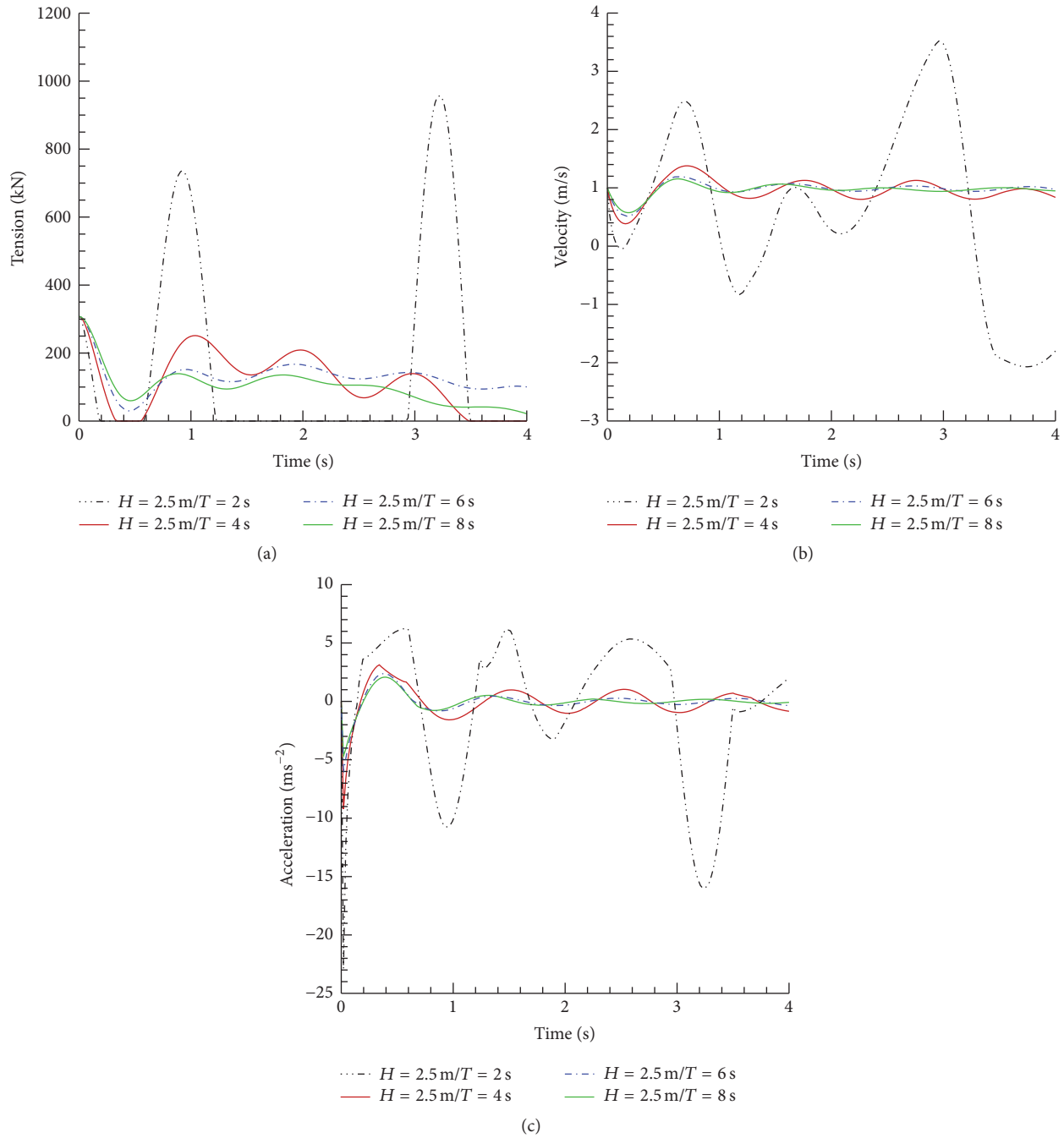
Acknowledgments

(a)

(b)

(c)
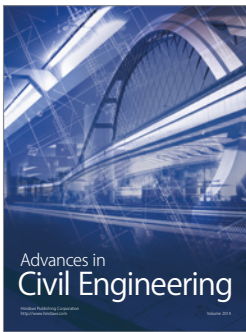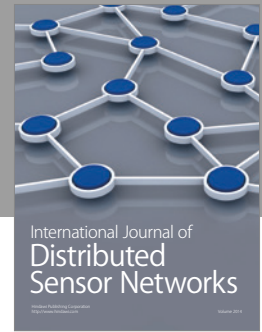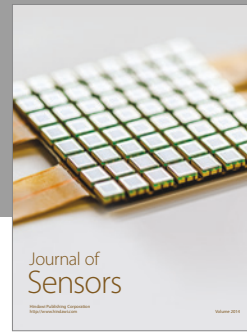
Figure 12: Influence of wave periods: (a) tension acting on the cylinder; (b) velocity of the cylinder; (c) acceleration of the cylinder.

References

[1] X. Li, C. Ye, C. Wang, C. Tao, and X. Xiao, "Chinese manned submersible JIAOLONG's scientific cruise in 2014-2015," in *Proceedings of the MTS/IEEE Washington, OCEANS 2015*, October 2015.

[2] T. Shimizu, Y. Yamamoto, N. Tenma, and H. Narita, "Electric-submersible-pump performance under methane/water/methane-hydrate pipe flows," in *Proceedings of the 25th International Ocean and Polar Engineering Conference, ISOPE 2015*, pp. 132–138, USA, June 2015.

[3] D.-J. Li, Y.-H. Chen, J.-G. Shi, and C.-J. Yang, "Autonomous underwater vehicle docking system for cabled ocean observatory network," *Ocean Engineering*, vol. 109, pp. 127–134, 2015.

[4] V. Karman, The impact of seaplane floats during landing. National Advisory Committee for Aeronautics, TN 321, pp.1-8, 1929.

[5] H. Wanger, "Trans phenomena associated with impacts and sliding on liquid surfaces," *Math Mechanics*, vol. 12, no. 4, pp. 193–215, 1932.

[6] O. M. Faltinsen, *Sea Loads on Ships and Offshore Structure*, Cambridge university press, 1993.

[7] H. Sun and O. M. Faltinsen, "Water impact of horizontal circular cylinders and cylindrical shells," *Applied Ocean Research*, vol. 28, no. 5, pp. 299–311, 2006.

[8] C. Mnasri, Z. Hafsia, M. Omri, and K. Maalel, "A moving grid model for simulation of free surface behavior induced by horizontal cylinders exit and entry," *Engineering Applications of Computational Fluid Mechanics*, vol. 4, no. 2, pp. 260–275, 2014.

[9] P. Ghadimi, A. Dashtimanesh, and S. R. Djeddi, "Study of water entry of circular cylinder by using analytical and numerical solutions," *Journal of the Brazilian Society of Mechanical Sciences & Engineering*, vol. 34, no. 3, pp. 225–232, 2012.

[10] A. Tassin, D. J. Piro, A. A. Korobkin, K. J. Maki, and M. J. Cooker, "Two-dimensional water entry and exit of a body whose shape varies in time," *Journal of Fluids and Structures*, vol. 40, pp. 317–336, 2013.

[11] A. Iranmanesh and M. Passandideh-Fard, "A three-dimensional numerical approach on water entry of a horizontal circular cylinder using the volume of fluid technique," *Ocean Engineering*, vol. 130, pp. 557–566, 2017.

[12] B. Bas, T. Bunnik, D. Honig, and G. Meskers, "A new simulation method for installation of subsea structures from the splash zone to the ultra deep," in *Proceedings of the DOT Conference*, New Orleans, La, USA, 2004.

[13] T. Bunnik and B. Buchner, "Numerical prediction of wave loads on subsea structures in the splash zone," in *Proceedings of the 14th International Offshore and Polar Engineering Conference (ISOPE)*, pp. 284–290, Toulon, France, May 2004.

[14] T. Bunnik, B. Buchner, and A. Veldman, "The use of a Volume of Fluid (VOF) method coupled to a time domain motion simulation to calculate the motions of a subsea structure lifted through the splash zone," in *Proceedings of the 25TH International Conference on Offshore Mechanics and Arctic Engineering, OMAE 2006*, Hamburg, Germany, June 2006.

[15] J. Y. Zhang, D. J. Li, X. Y. Gao, Q. C. Meng, C. J. Yang, and Y. Chen, "Simulation analysis of deployment and retrieval of junction box used in cabled seafloor observatory," *Ship Engineering*, vol. 32, no. 6, pp. 53–59, 2010 (Chinese).

[16] W.-H. Wang and Y.-Y. Wang, "An essential solution of water entry problems and its engineering applications," *Journal of Marine Science and Application*, vol. 9, no. 3, pp. 268–273, 2010.

[17] P. Ryzhakov, R. Rossi, A. Viña, and E. Oñate, "Modelling and simulation of the sea-landing of aerial vehicles using the Particle Finite Element Method," *Ocean Engineering*, vol. 66, pp. 92–100, 2013.

[18] P. Wen and W. Qiu, "Solving 2-D water entry problems with a CIP method and a parallel computing algorithm," *Marine Systems Ocean Technology*, vol. 11, no. 1-2, p. 1, 2016.

[19] T. Zhang, D. Li, and C. Yang, "Study on impact process of AUV underwater docking with a cone-shaped dock," *Ocean Engineering*, vol. 130, pp. 176–187, 2017.

[20] J. M. Niedzwecki and S. K. Thampi, "Snap loading of marine cable systems," *Applied Ocean Research*, vol. 13, no. 1, pp. 2–11, 1991.

[21] K. W. Thurston, R. C. Swanson, and F. Kopp, "Statistical characterization of slacking and snap loading during offshore lifting and lowering in a wave environment," in *Proceedings of the ASME 2011 30th International Conference on Ocean, Offshore and Arctic Engineering, OMAE2011*, pp. 269–277, nld, June 2011.

[22] W. Lu, F. Ge, L. Wang, X. Wu, and Y. Hong, "On the slack phenomena and snap force in tethers of submerged floating tunnels under wave conditions," *Marine Structures*, vol. 24, no. 4, pp. 358–376, 2011.

[23] A. Selvåg, Wave impact forces on complex structures during lowering through the splash zone, Master's Thesis, Norw. Univ. Sci. Technol., Trondheim, 2013.

[24] M. Wu, Dynamic analysis of a subsea module during splash-zone transit, Master's Thesis, Norw. Univ. Sci. Technol., Trondheim, 2013.

[25] M. Valen, Launch and recovery of ROV: Investigation of operational limit from DNV Recommended Practices and time domain simulations in SIMO, Master's Thesis, Norwegian Norw. Univ. Sci. Technol., Trondheim, 2010.

[26] R. B. Gordon, G. Grytøyr, and M. Dhaigude, "Modeling suction pile lowering through the splash zone," in *Proceedings of the ASME 32nd International Conference on Ocean, Offshore and Arctic Engineering, OMAE 2013*, Nantes, France, June 2013.

[27] T. Jacobsen and B. J. Leira, "Numerical and experimental studies of submerged towing of a subsea template," *Ocean Engineering*, vol. 42, pp. 147–154, 2012.

[28] L. Li, Z. Gao, T. Moan, and H. Ormberg, "Analysis of lifting operation of a monopile for an offshore wind turbine considering vessel shielding effects," *Marine Structures*, vol. 39, pp. 287–314, 2014.

[29] L. Li, Z. Gao, and T. Moan, "Comparative study of lifting operations of offshore wind turbine monopile and jacket substructures considering vessel shielding effects," in *Proceedings of the Twenty-fifth International Ocean and Polar Engineering Conference*, pp. 1290–1298, USA, 2015.

[30] H. Xiaozhou and L. Shaojun, "Numerical investigation of dynamic response of deploying system during a circular cylinder lowering through air-water interface," *International Journal of Fluid Mechanics Research*, vol. 42, no. 3, pp. 191–205, 2015.

[31] B. E. Launder and D. B. Spalding, *Lectures in Mathematical Models of Turbulence*, Academic Press, London, England, 1972.